

Multiscale Morphological Analysis of the Atherosclerotic Carotid Plaque

E. Kyriacou^{1,3}, M.S. Pattichis², C.I. Christodoulou^{1,3}, C.S. Pattichis³, S. Kakkos⁴, A. Nicolaides^{1,3,4}
¹Department of Computer Science, University of Cyprus, 75 Kallipoleos Str., P.O.Box 20578, 1678 Nicosia, Cyprus

{ekyriac, cschr2, pattichi}@ucy.ac.cy

²Department of Electrical and Computer Engineering, University of New Mexico, Albuquerque, USA
pattichis@ece.unm.edu

³Cyprus Institute of Neurology and Genetics, Nicosia, Cyprus
anicolai@cing.ac.cy

⁴Department of Vascular Surgery, Faculty of Medicine, Imperial College, University of London, London, UK
s.kakkos@imperial.ac.uk

Abstract—The aim of this paper was to investigate the usefulness of multiscale morphological analysis in the assessment of atherosclerotic carotid plaques. Ultrasound images were recorded from 137 asymptomatic and 137 symptomatic plaques and were converted to binary images at low, middle and high intensity intervals based on structural morphology. Low images represent low intensity regions corresponding to blood, thrombus, lipid or hemorrhage, whereas high images describe the collagen and calcified components of the plaque. Middle image describe image regions that fall between low and high components. The morphological pattern spectra were computed and several classifiers like the K-Nearest Neighbor (KNN), the Probabilistic Neural Network (PNN), and the Support Vector Machine (SVM) were evaluated for classifying these spectra into two classes: asymptomatic or symptomatic. The highest diagnostic yield achieved was 67% that is slightly lower than texture analysis carried out on the same data set.

Keywords— Ultrasound plaque imaging, morphology, multiscale analysis, texture analysis, stroke assessment,

I. INTRODUCTION

High-resolution ultrasound has made possible the noninvasive visualization of the carotid bifurcation and for that reason it has been extensively used in the study of arterial wall changes; these include measurement of the thickness of the intima media complex (IMT), estimation of the severity of stenosis due to atherosclerotic plaques and plaque characterization [1].

During the last decade, the introduction of computer aided methods and image standardization has improved the objective assessment of carotid plaque echogenicity, and heterogeneity [2], and has largely replaced subjective (visual) assessment [1], that had been criticized for its relatively poor reproducibility [3].

Previous studies investigated the usefulness of texture analysis [4]-[8], and more recently, morphological analysis was also used [6]-[8] towards the development of a Computer Aided Diagnostic (CAD) system for the classification of asymptomatic and symptomatic atherosclerotic plaques. These studies gave promising results. The objective of this study was to investigate the

usefulness of multiscale morphological analysis in the aforementioned classification, and compare the findings with other studies.

In this paper, section II describes the material, image acquisition, normalization and segmentation of plaque images. Sections III and IV describe the multiscale morphological analysis and the classification algorithms, respectively. Section V gives the results and section VI the concluding remarks.

II. MATERIAL, IMAGE ACQUISITION, NORMALIZATION AND SEGMENTATION

A total of 274 carotid plaque ultrasound images (137 asymptomatic plaques and 137 symptomatic plaques associated with retinal or hemispheric symptoms (33 stroke, 60 TIA, and 44 AF). Patients with cardioembolic symptoms or distant symptoms (> 6 months) were excluded from the study. Asymptomatic plaques were truly asymptomatic if they had never been associated with symptoms in the past associated with retinal or hemispheric symptoms (Stroke, TIA or AF), i.e. unstable plaques.

The ultrasound images were collected in the Irvine Laboratory for Cardiovascular Investigation and Research, Saint Mary's Hospital, UK, using an ATL (model HDI 3000 - Advanced Technology Laboratories, Seattle, USA) duplex scanner with a linear broadband width 7-4 MHz (multifrequency) transducer, at approximately a resolution of 20 pix/mm.

The images were normalized manually by adjusting the image linearly so that the median gray level value of blood was in the range of 0-5, and the median gray level of adventitia (artery wall) was in the range of 180-190 [9]. The scale of the gray level of the images ranged from 0 to 255. This normalization (i.e. using blood and adventitia as reference points) was necessary in order to extract comparable measurements in case of processing images obtained by different operators or different equipment [9].

The plaque identification and segmentation tasks are quite difficult and were carried out manually by a physician or vascular ultrasonographer who are experienced in scanning. The main difficulties are due to the fact that the

plaque edges cannot be distinguished from blood based on brightness level difference, or using only texture features, or other measures. Also calcification and acoustic shadows make the problem more complex. Thus, acoustic shadows were excluded. A system for facilitating the automated segmentation of carotid plaque based on snakes is currently under development by our group [10].

III. MULTISCALE MORPHOLOGICAL ANALYSIS

Morphological features are motivated from the need to study the basic structure of the plaque. We used a multi-level approach where the image intensity was thresholded at three different levels to generate binary images corresponding to different structural elements in the images (see (1)). The first set of binary images (*lowimg*) represents low intensity values that are considered to be difficult to see against low intensity backgrounds. Structurally, these low intensity regions correspond to blood, thrombus, lipid or hemorrhage. Structurally, binary images corresponding to high intensity values (*highimg*) describe the collagen and calcified components of the plaques. The second set of binary images (*middleimg*) describes image regions that fall between low and high intensity components. For each plaque image *img*, we used:

$$\begin{aligned} \text{lowimg} &= \{(x,y) \text{ such that } \text{img}(x,y) < 25\} \\ \text{middleimg} &= \{(x,y) \text{ such that } 25 \leq \text{img}(x,y) \leq 50\} \\ \text{highimg} &= \{(x,y) \text{ such that } 50 < \text{img}(x,y)\} \end{aligned} \quad (1)$$

to generate the binary images for the analysis.

To recognize the morphological features of the image components, we comment on the topology of the binary blob (white) components. The blob-components in the *lowimg* and the *highimg* are made up of solid (without holes) components. On the other hand, the blob-components of the *middleimg* are filled with holes that correspond to the lipid cores of the *highimg*.

The morphological pattern spectra defined in terms of the binary images aim at describing the different size components that are of diagnostic interest. For example, if the plaque image is captured as a single white component in the *lowimg* or the *highimg*, then the plaque structure is considered to be stable with little chance for rupture. Also, if the lipid core regions are made up of small scattered components, these are not considered to be dangerous.

The most dangerous cases occur when the intermediate regions in the *middleimg* appear to be very thin. A somewhat less dangerous case occurs when these regions are relatively thick.

In morphological image processing, we proceed to characterize the size distributions of both the blob-components which appear white, and the hole-components which appear black. For describing these components, we consider a cross structural element ('+') that does not exhibit

any directional selectivity. The size distribution measures the presence of blob components of radius proportional to the positive index of the Pattern Spectrum. Similarly, the size distribution of the presence of holes is proportional to the negative index of the Pattern Spectrum. We will next provide a mathematical description of the Pattern Spectrum.

We consider pattern spectra based on a flat '+' structural element *B*, made up of 5 pixels. The Pattern Spectrum is defined in terms of the Discrete Size Transform (DST).

We define the DST using [11], [12]:

$f \rightarrow (\dots, d_{-k}(f; B), \dots, d_{-1}(f; B), d_0(f; B), \dots, d_1(f; B), \dots, d_k(f; B), \dots)$ where

$$d_k(f; B) = \begin{cases} f \circ k B - f \circ (k+1) B, & k \geq 0 \\ f \bullet |k| B - f \bullet (|k|-1) B, & k \leq 0 \end{cases},$$

o denotes an open operation, and *•* denotes the close operation. The binary DST is a multi-resolution image decomposition scheme, which decomposes an image *f* into residual images $f \circ k B - f \circ (k+1) B$, for $k > 0$, and $f \bullet |k| B - f \bullet (|k|-1) B$ for $k < 0$. The pattern spectrum of a binary image *f*, in terms of a structural element *B*, is given by:

$$P_{f;B}(k) = \|d_k(f; B)\| = \begin{cases} \|f \circ k B - f \circ (k+1) B\|, & k \geq 0 \\ \|f \bullet |k| B - f \bullet (|k|-1) B\|, & k \leq 0 \end{cases}$$

where

$$\|f\| = \sum_{x,y} f(x,y), \quad f(x,y) \geq 0.$$

We note that in the limit, as $k \rightarrow \infty$, we have that the resulting image $f \circ k B - f \circ (k+1) B$ converges to the zero image. Also, we note that with increasing values of *k*, $f \circ k B$ is a subset of the original image. For $k \geq 0$, we may thus normalize the Pattern Spectrum by dividing by the norm of the original image $\|f\|$. Similarly, as $k \rightarrow \infty$, by using constant extensions for extending binary images at their boundaries, $\|f \bullet k B\|$ converges to $NM \max f(x,y)$, where it is assumed that the image is of size *N* by *M*. Hence, for $k < 0$, we can normalize the pattern spectrum by dividing by $NM \max f(x,y) - \|f\|$. Thus, to eliminate undesired variations, all the pattern spectra were normalized. As mentioned earlier the pattern spectra were computed for three binary images, corresponding to low, middle, and high image intensity values.

IV. CLASSIFICATION TECHNIQUES

The diagnostic performance of the morphological features was evaluated with three different classifiers: the K-Nearest Neighbor (KNN), the Probabilistic Neural Network (PNN), and the Support Vector Machine (SVM). These classifiers were trained to classify the morphology features into two classes: i) asymptomatic plaques or ii) symptomatic plaques associated with retinal or hemispheric symptoms (Stroke, TIA or AF), i.e. unstable plaques.

The statistical pattern recognition KNN classifier was investigated using the Euclidean distance and $k=7$. Moreover, classifiers based on PNN [13] and SVM with Gaussian Radial Basis Function (RBF) kernels were investigated [14].

The leave-one-out estimate was used for validating the classification models. A total of 274 subsets of size 273 were used for training the classifiers, and the performance of the classifiers was evaluated on the remaining one subset.

V. RESULTS

The mean morphological pattern spectra that gave the best classification results are summarized in Fig. 1. For plaque image regions with low image intensity, we compute the mean cumulative distribution functions (*cdf*) for the openings, which constitute the positive part of the pattern spectrum, (Fig. 1.a) and the closings, for the negative part of the spectrum, (Fig. 1.b). For plaque image regions with image intensity in the middle range, we show the mean probability density function for the closings in Fig. 1c. The spectra are plotted against the radius (in mm) of the circular structural element that was used.

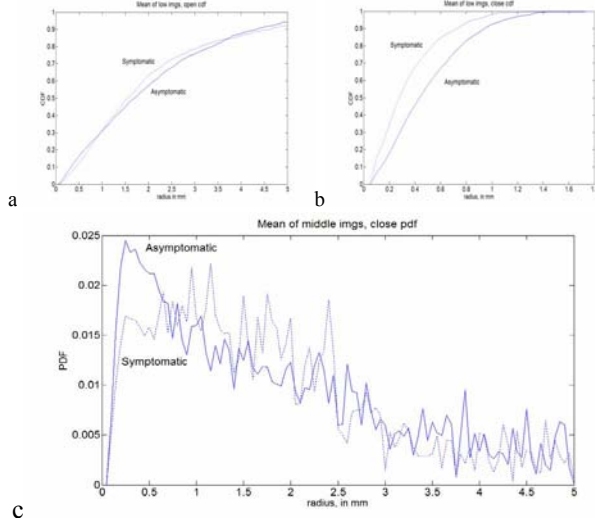


Fig. 1. a) Mean cumulative distribution function (*cdf*) plots for images thresholded at a low threshold, for the openings. The asymptomatic plot is plotted with a solid line, while the symptomatic plot is plotted with a dotted line b) Mean cumulative distribution function (*cdf*) plots for images thresholded at a low threshold, for the closings. The asymptomatic plot is plotted with a solid line, while the symptomatic plot is plotted with a dotted line c) Mean probability density function (*pdf*) plots for images thresholded at the middle range, for the closings. The asymptomatic plot is plotted with a solid line, while the symptomatic plot is plotted with a dotted line

From Fig 1.b we see that the mean symptomatic (close) *cdf* is above the mean asymptomatic *cdf*. We say that the symptomatic *cdf* is *stochastically larger* than the asymptomatic *cdf*. This implies that dark regions in the symptomatic cases were somewhat closer together, leaving smaller "holes" between the dark regions. Another important feature of this figure is that all the "holes" were found to be of a diameter that is less than 3.6mm ($3.6\text{mm} = 2 \times 1.8\text{mm}$).

From Fig. 1.b, we see that the mean cumulative distribution functions for the (open) *cdfs* are very close between the symptomatic and asymptomatic cases. From the graph intersections around 1mm and 3.6mm, we infer that the dark regions in the symptomatic plaques have shown increased presence within these two sizes.

From Fig. 1.c, we can see that the mean (close) probability density function for the asymptomatic plaques lies well above the symptomatic plaques for radii in the neighborhood of 1mm. This implies that mid-range intensity regions below 2mm diameter ($2\text{mm} = 2 \times 1\text{mm}$) showed a stronger presence in the asymptomatic cases.

Morphology features for low, medium and high images, as described in section III were used in order to classify images using the KNN, PNN and SVM classifiers. The dimensionality of the features vector was reduced using PCA to account for 98% of the total variance. Table I illustrates the results from these classifiers and the different morphology sets. The use of PNN and SVM classifiers significantly improved results, compared to those of KNN. For the PNN classifier, the highest diagnostic yield (DY) of 62% was achieved using the left part of the pattern spectra (close) from the mid intensity images with PCA. For the SVM classifier, the highest DY was achieved for the same pattern spectra as for PNN with a DY of 67%.

VI. CONCLUDING REMARKS

Morphological features help us understand the interrelations among different intensity regions. We have examined morphological results from dark, mid-range, and high intensity regions. We have found that there was significant overlap between the pattern spectra coming from symptomatic and asymptomatic plaques. Furthermore, as we expected, probability density function (*pdf*) estimates were visually verified to be noisier than cumulative distribution function estimates. For larger morphological components, the *pdf* started to drop, and the variance in the estimates increased significantly. Thus, most of the discriminating power was concentrated in the smaller components, around a radius of 1mm.

The results in this study are comparable with previous work carried out with different datasets [5]-[8], as well as by another group [4]. In [5], the highest diagnostic yield achieved was 73% using the self-organizing map (SOM) classifier and multiple texture feature sets and combining techniques. In [6], it was shown that morphological features compare well with the most successful texture feature sets and provide additional information for the identification of

individuals at risk of stroke. The combination of morphology and texture features slightly increases the diagnostic yield [6]-[8].

TABLE I
PERCENTAGE DIAGNOSTIC YIELD (DY%) OF MORPHOLOGICAL FEATURES USING KNN $k=7$, PNN, AND SVM CLASSIFIERS, FOR THE CLASSIFICATION OF TWO CLASSES OF PLAQUE (FOR 137 SYMPTOMATIC AND 137 ASYMPTOMATIC PLAQUES)

Morphology features	KNN ($k=7$) DY %		PNN DY%		SVM DY%
	Orig.	PCA (98%)	Orig.	PCA (98%)	PCA (98%)
Low image					
pdf_open	45	52	55	57	63
cdf_open	55	52	55	59	64
pdf_close	52	55	60	59	62
cdf_close	50	50	51	52	64
Medium Image					
pdf_open	55	54	60	53	52
cdf_open	51	53	58	58	63
pdf_close	46	46	56	62	67
cdf_close	55	56	58	58	63
High Image					
pdf_open	56	56	55	49	58
cdf_open	60	64	55	54	54
pdf_close	48	48	53	57	62
cdf_close	56	57	53	59	55

Future work will investigate the performance of texture and morphology feature sets on larger data sets, as well as how the diagnostic yield is improved with the combination of clinical and other features.

ACKNOWLEDGMENT

This work was funded through the projects Integrated System for the Support of the Diagnosis for the Risk of Stroke (IASIS), and Integrated System for the Evaluation of Ultrasound Imaging of the Carotid Artery (TALOS), of the Research Promotion Foundation of Cyprus.

REFERENCES

- [1] Belcaro G, Nicolaidis AN, Laurora G, et al. Ultrasound morphology classification of the arterial wall and cardiovascular events in a 6-year follow-up study. *Arterioscler Thromb Vasc Biol* 1996; 16:851-6.
- [2] El-Barghouti N, Nicolaidis AN, Tegos T, et al. The relative effect of carotid plaque heterogeneity and echogenicity on ipsilateral cerebral infarction and symptoms of cerebrovascular disease. *Int Angiol* 1996; 15:300-6.
- [3] Arnold JAC, Modaresi KB, Thomas N, et al. Carotid plaque characterization by duplex scanning. Observer error may undermine current clinical trials. *Stroke* 1999; 30:61-5.
- [4] Wilhelm J.E., Gronholdt L.M., Wiebe B., Jespersen S.K., Hansen L.K., Sillesen H., "Quantitative Analysis of Ultrasound B-Mode Images of Carotid Atherosclerotic Plaque: Correlation with Visual Classification and Histological Examination", *IEEE Transactions on Medical Imaging*, Vol. 17, No. 6, pp.910-922, December 1998.
- [5] Christodoulou CI, Pattichis CS, Pantziaris M, Nicolaidis A. Texture Based Classification of Atherosclerotic Carotid Plaques. *IEEE Transactions on Medical Imaging*. 2003; 22: 902-912.
- [6] Christodoulou CI, Kyriacou E, Pattichis MS, Pattichis CS, Nicolaidis A. A Comparative Study of Morphological and other Texture Features for the Characterization of Atherosclerotic Carotid Plaques. *Computer Analysis of Images and Patterns, 10th International Conference CAIP'2004*, Groningen, The Netherlands. Springer-Verlag . 2004 August 25-27; 503-511.
- [7] Christodoulou CI, Pattichis CS, Kyriacou E, Pattichis M.S., Pantziaris M, Nicolaidis A. Texture and Morphological Analysis of Ultrasound Images of the Carotid Plaque for the Assessment of Stroke. *Applied Medical Image Analysis Methods*. ed. by L. Costaridou, CRC Press, pp. 87-135, 2005.
- [8] Kyriacou E., Pattichis M.S., Christodoulou C., Pattichis C.S., Kakkos S., Nicolaidis A., *Ultrasound Imaging in the Analysis of Carotid Plaque Morphology for the Assessment of Stroke*, in *Plaque Characterization using Multimodality Imaging: Pixel to Molecular*, Ed. by J.S. Suri, C. Yuan, D.L. Wilson, S. Laxminarayan, IOS Press, 2005.
- [9] Tegos TJ, Sametaj MM, Nicolaidis AN et al. Comparability of the ultrasonic tissue characteristics of carotid plaques. *J Ultrasound Med* 2000; 19:399-407.
- [10] Loizou C., Pattichis C., Istepanian R., Pantziaris M., Nicolaidis A., *Atherosclerotic Carotid Plaque Segmentation*, Proceedings of the 26th Annual International Conference of the IEEE Engineering in Medicine and Biology Society, 1-5 September, San Francisco, California, USA, 2004, 4 pages.
- [11] Dougherty ER. *An Introduction to Morphological Image Processing*, Bellingham. Washington. SPIE Optical Engineering Press 1992.
- [12] Maragos P. Pattern spectrum and multiscale shape representation. *IEEE Trans. on Pattern Analysis and Machine Intelligence*.1989; 11:701 715.
- [13] Specht DF. Probabilistic Neural Networks. *INNS Neural Networks*. 1990; 3(1):109-118.
- [14] Joachims T. 11 in: *Making large-Scale SVM Learning Practical*. *Advances in Kernel Methods - Support Vector Learning*, B. Schölkopf and C. Burges and A. Smola (ed.). MIT Press. 1999.